PAPER

Influence of liquid conductance on the temporal evolution of self-organization patterns in atmospheric pressure DC glow discharges

To cite this article: Bhagirath Ghimire et al 2023 Phys. Scr. 98 095602

View the article online for updates and enhancements.

You may also like

- What Are the Effective Reactants in the Plasma-Induced Wastewater Treatment? Bangbang He, Xinning Gong, Xin Wang et al
- Quantification of plasma produced OH and electron fluxes at the liquid anode and their role in plasma driven solution electrochemistry

Yuanfu Yue, Stephen Exarhos, Jaehyun Nam et al.

 A review of plasma—liquid interactions for nanomaterial synthesis
Qiang Chen, Junshuai Li and Yongfeng Li

Physica Scripta



12 May 2023

REVISED 21 July 2023

ACCEPTED FOR PUBLICATION 27 July 2023

PUBLISHED

7 August 2023

PAPER

Influence of liquid conductance on the temporal evolution of selforganization patterns in atmospheric pressure DC glow discharges

Bhagirath Ghimire^{1,2}, Vladimir I Kolobov^{1,3} and Kunning G Xu²

- Center for Space Plasma and Aeronomic Research, University of Alabama in Huntsville, Huntsville AL, 35899 United States of America
- Department of Mechanical and Aerospace Engineering, University of Alabama in Huntsville, Huntsville AL, 35899 United States of America
- CFD Research Corporation, Huntsville, AL, 35806 United States of America

E-mail: bhagirath.ghimire@uah.edu and gabe.xu@uah.edu

Keywords: low temperature plasmas, liquid-anode discharges, self-organized patterns, optical emission spectroscopy, conductivity, DC plasmas, plasma-liquid interactions

Abstract

Self-Organized Patterns (SOPs) at plasma-liquid interface in atmospheric pressure plasma discharges refer to the formation of intricate and puzzling structures due to the interplay of electrodynamic and hydrodynamic processes. Studies conducted to date have shown that this phenomenon results in the formation of distinctive patterns such as circular ring, star, gear, dots, spikes, etc., and primarily depends on working gas, electrolyte type, gap distance, current, conductivity, etc. However, an adequate understanding of how these patterns change from one type to another is still not available. This study aims to elucidate the influence of initial liquid conductance (σ_i) on the temporal evolution of SOPs in liquid-anode discharges. The discharge was generated in a pin-to-liquid anode configuration at a constant helium (He) flow rate of 500 sccm and DC applied voltage of 6 kV at a gap distance of 12 mm. Through the gradual increment of σ_i from 1.8 μ S to 4820 μ S, we observe that the trend in the evolution of SOPS takes place as solid discs, spikes, dots, rings, double rings, and stars. The continuous formation of reactive species onto the liquid anode in all conductive solutions results in a decrease in pH, an increase in bulk liquid temperature, and an increase in total dissolved solutes, and these have been confirmed through experimental measurements. Observations using optical emission spectroscopy show that the electrons at the plasma-liquid interface participate in the reduction of cations followed by their excitation & ionization due to which electron density as well as emissions from excited species (mainly hydroxyl radicals & excited nitrogen) decrease with time. Our investigation provides experimental evidence on the presence of cations at the plasma-liquid interface required for SOP formation.

1. Introduction

Self-organized patterns (SOPs) at plasma-liquid interfaces refer to the formation of spatially non-uniform, dynamic structures that arise from the interaction between a gaseous plasma and a liquid. Plasma interactions with liquids have given rise to several emerging applications including nanomaterial synthesis, surface modification, water treatment, sterilization, material recycling, decontamination of toxic compounds and medicine [1-4]. The SOPs in discharges with liquid anodes can be of various shapes, patterns, or structures. This phenomenon is a complex, multi-phase process involving a combination of electrodynamic and hydrodynamic

During the last decade, the formation of SOPs in liquid-anode discharges has been extensively investigated using both experimental and modeling techniques [5-10]. Experimental observations have mainly been done through the variation of plasma operating parameters (such as applied voltage, current, working gas, gap distance, etc) and the properties of liquid solution (such as conductivity, pH, and electrolyte type). Shirai et al

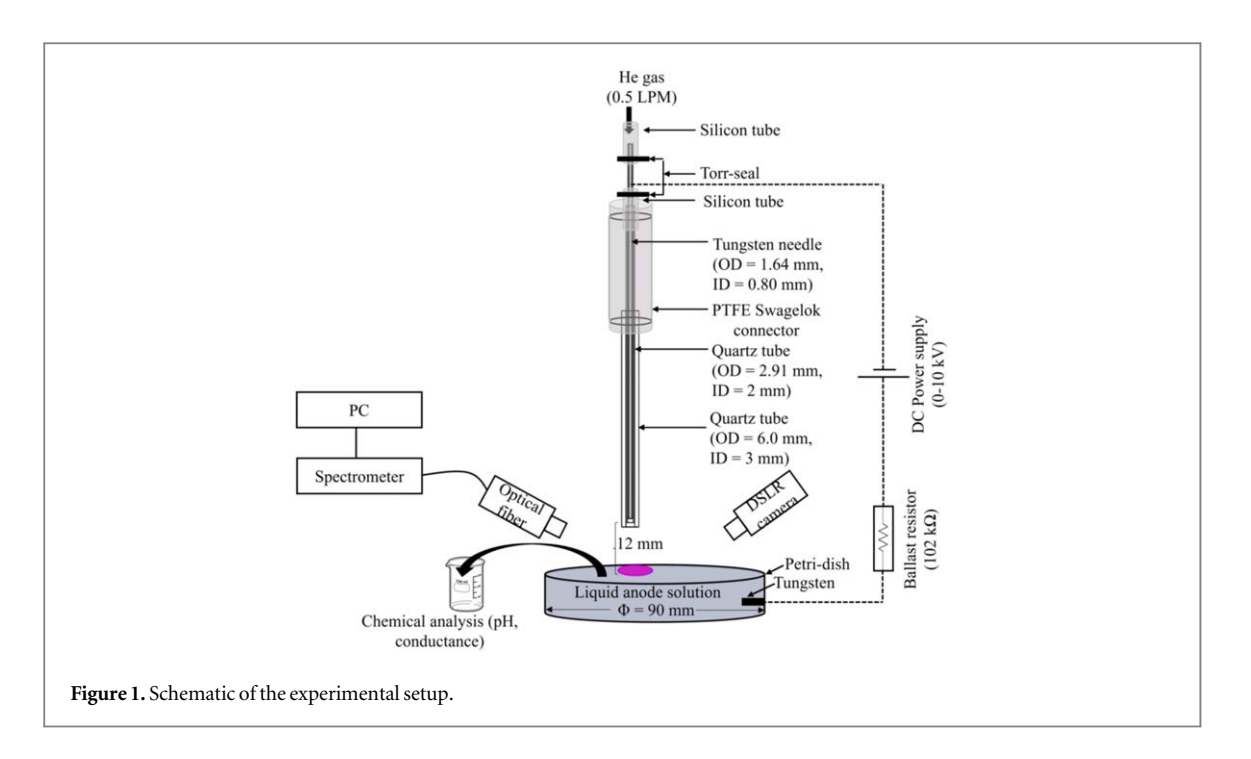
investigated the dependence of gap distance, the presence of oxygen, applied potential, and the liquid temperature [3, 11–16] on the formation of SOPs. Different patterns such as wedge-shaped, annular-shaped, and spot have been observed by variations of these parameters. Their observations suggest that the addition of electronegative gases such as oxygen in the discharge region is a key factor to control the formation of SOPs [16]. The presence of negative ions in discharges have been suggested to lead to a type of ionization instability, which may play a role in the formation of patterned anode spots. Li et al reported different patterns including diffusedisk, single-ring, disk-ring, wheel-spokes, and radial stripes by using a miniature argon flow [17]. The formation of these patterns is attributed to the movement and periodic formation/collapse of anode spots due to the presence of electronegative species like atomic oxygen (O), nitric oxide (NO), hydroxyl radical (OH), and amine (NH) which were also detected through optical emission spectroscopy. This observation supports the essential role of electronegative gases as proposed by Shirai et al on the formation of SOPs [13]. Zhang and Dufour observed that the formation of SOPS is dependent on the type of electrolyte solution and its conductivity [18]. Differences in the size of SOPs and discretization were observed when the liquid anode was set to sulphuric acid and hydrochloric acid at the same conductivities for the discharge operated in ambient air. Their report suggests that the electronegativity of the anion could play a key role in the formation of SOPs. This hypothesis contrasts the recent observation made by Srivastava et al [19]. Although, they also observe the dependence of SOP on liquid conductivity and electrolyte type, the condition for pattern formation is ascribed to the presence of cations for which the corresponding metal atom has low ionization energy. Kovach et al also studied the behavior of pattern formation with 13 different liquid anode electrolytes with different ionic strengths [20]. The pattern evolution in their case did not appreciably depend on ionic strengths. It should be understood that the molecular concentrations used in [20] were relatively high and initial liquid conductivities among different electrolytes were not the same which could be a possible reason for not observing the differences. In addition, numerical modeling and simulations carried out by Islamov and Gulamov indicate effects of electron-ion recombination on pattern formation [21]. Modeling studies of the liquid boundary layer by Rumbach et al to predict the formation of patterns on a liquid anode surface suggest that the size and structure of the patterns depend on the plasma current and the conductivity of the liquid anode [22].

Despite the extensive number of published literatures, the transition among different types of patterns and a clear understanding on their behavior is still not available. In this article, we investigate the influence of initial liquid conductivity on the formation of SOPs at the plasma-liquid interface. This has been analyzed through the measurement of chemical properties of the anode solution and optical emission spectroscopy.

2. Experimental setup

Figure 1 shows the schematic of the experimental setup. The plasma source is designed by inserting a tungsten needle electrode (inner diameter, ID = 0.80 mm, outer diameter, OD = 1.64 mm) inside both ends open quartz tube (ID = 2 mm, OD = 2.91 mm) and inserting the assembly inside a straight Swagelok connector. Two silicon tubings (OD = 6 mm) separated by a distance of 1 cm surround the needle electrode on the top portion. The negative terminal of the power supply is connected to the needle electrode at this point. The top silicon tubing is fitted to another straight Swagelok connector through which helium gas at a flow rate of 0.5 standard liters per minute (SLPM) flows into the discharge region. The region of the silicon tubing below / above swagelok connector(s) is sealed by torr-seal. The bottom portion of the internal quartz tube and needle electrode assembly is further inserted inside a second quartz tube (OD = 6 mm, ID = 3 mm, length = 10 cm). The distance between the end of the needle electrode (as well as the internal quartz tube) and the end of the second quartz tube is 3 mm. The flow of He gas into the discharge region is controlled using a mass flow controller (Model: GE50A013503SBV020, MKS Instruments Inc.). The anode is a liquid solution (distilled water or distilled water with dissolved sodium chloride (NaCl) of different initial conductivity, volume = 120 ml) filled inside a quartz petri-dish (diameter = 90 mm, height = 20 mm). A tungsten electrode (diameter = 1 mm) remained in contact with the liquid solution through a small hole drilled and sealed by torr-real at the bottom of the petri-dish. Plasma was generated by connecting the positive terminal of the DC power supply (Model no: AU-10P60, Matsusada Inc.) to the liquid solution through a $102 \text{ k}\Omega$ ballast resistor (power rating: 100W) and the negative terminal connected to the upstream tungsten needle electrode. The ballast resistor limits the current in the discharge and prevents the transition to arc mode. The gap distance (g) between the nozzle of the quartz tube and anode solution was set to 12 mm.

The patterns formed at the plasma-liquid interface during the discharge process were recorded using a DSLR camera (Nikon D5500) placed at an inclination of 45°. The images were recorded using the continuous shoot function at an interval of every 60 seconds and the plasma was operated continuously until ten minutes. Due to the formation (and accumulation) of reactive oxygen and nitrogen species (RONS) inside the liquid solution, the properties of the liquid solution changed with time. This was analyzed through the measurement of



conductance, pH and total dissolved solutes (TDS) using a Zentest liquid probe (Model no: LLC-AI3719 PC60-Z, Apera Instruments) before and after discharge ignition. Optical emission spectra of the SOPs were recorded using a 0.5 m Princeton Instruments SP2500 spectrometer coupled to a PI-MAX4 1024×256 pixel ICCD camera as well as Avantes spectrometer (Model no: AvaSpec-ULS4096CL-EVO). SP2500 spectrometer was calibrated in wavelength and intensity using the manufacturer-provided calibration lamps (Intellical, Princeton Instruments) while the Avantes spectrometer was factory calibrated. The spectra recorded with SP2500 spectrometer were used for the calculation of electron density. The change in optical emission intensities from different species in the range of 200-900 nm were analysed from the spectra recorded with Avantes spectrometer. The current values during the discharge were obtained from the digital display of the DC power supply.

3. Results and discussion

The results in this work are presented to show how the initial liquid conductance influences the formation of SOPs and how this induces a change in liquid chemical properties of the such as conductance, total dissolved solute, pH, etc with time. The formation of SOPs at different plasma ignition time are then correlated with the emission from different species at the plasma-liquid interface.

3.1. Effect of initial liquid conductance (σ_i)

The patterns observed with increasing σ_i 's from 1.8 μ S—4.8 mS are shown in figure 2. The conductance of the liquid solution was adjusted by dissolving NaCl in distilled water. The images were recorded at an interval of every sixty seconds and until 10 mins of plasma operation. For distilled water ($\sigma_i = 1.8 \,\mu\text{S}$), the plasma was very unstable during the first 60 seconds. During the second minute, a clear circular pattern with a bright emission was observed on the water surface. The intensity of this pattern decreased at 3-4 mins and closely spaced hairshaped structures filled the circle. At t = 6-7 mins, a gear-shaped pattern is formed on the water surface. The spacing between the individual gears increases with plasma ignition time. The conductance after t = 10 mins reaches 203 μ S, resulting in an increase by \approx 112 times. For the liquid solution with σ_i of 101.8 μ S, the plasma started with closely spaced hair-like structures forming a circular pattern and (unlike $\sigma_i = 1.8 \,\mu\text{S}$) the discharge was stable since the plasma was turned on. With the increase in plasma ignition time, the conductance of the solution increased and the spacing between the hair-shaped structures also increased giving rise to gear-shaped patterns. This was accompanied by the increased spacing between the individual gears as the plasma ignition time increased (quite similar to $\sigma_i = 1.8 \,\mu\text{S}$). After 10 mins of plasma operation, the conductance of the liquid solution reached 318 μ S, resulting in an increase by 2.12 times w.r.t. initial liquid conductance. For $\sigma_i = 191.6 \,\mu$ S, a similar behavior as $\sigma_i = 101.8 \,\mu\text{S}$ was observed but the spacing between the individual hair-like structures or gears increased with plasma ignition time. The final conductance of the solution was higher by 1.25 times as compared to the initial liquid conductance. Upon further increasing the initial liquid conductance, the

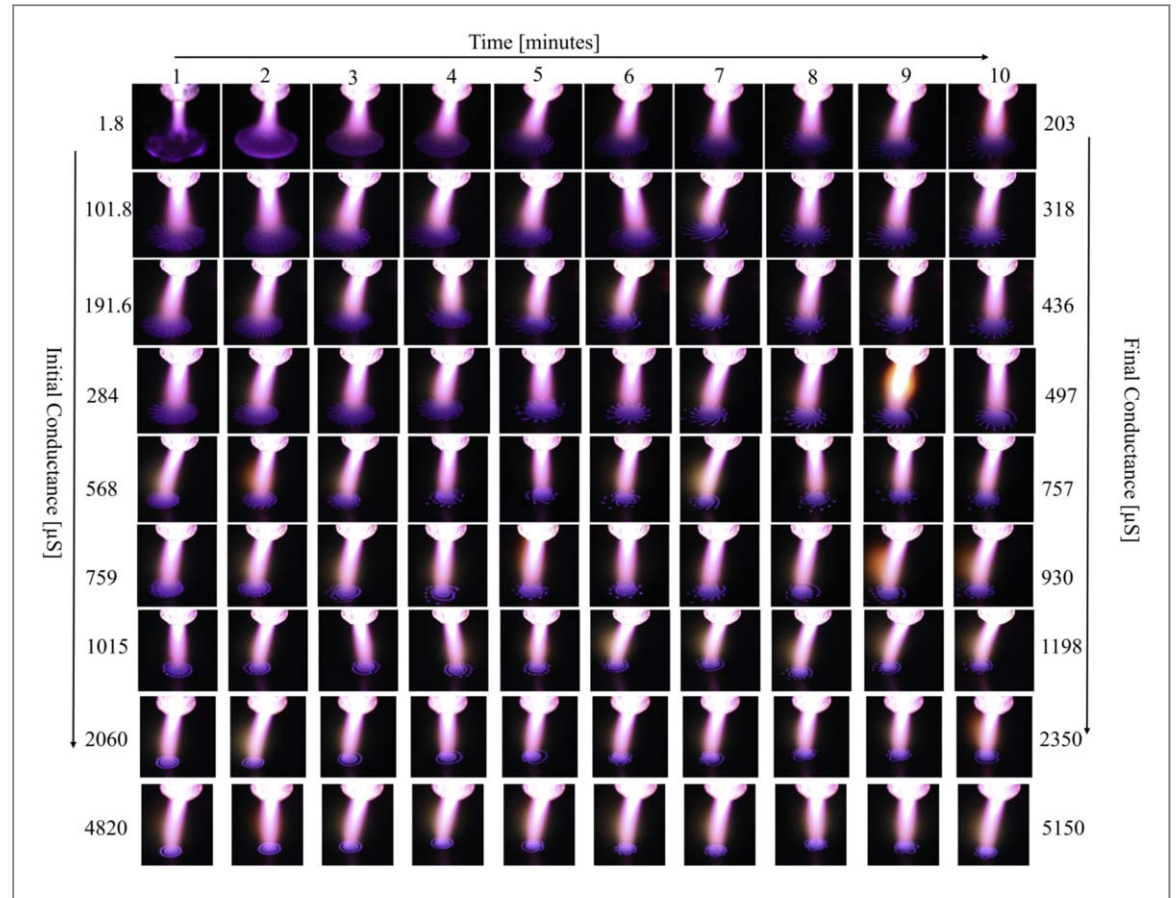


Figure 2. Temporal evolution of SOPs at the plasma-water interface for different σ_i 's (applied voltage = 6 kV DC, He flow rate = 0.5 SLPM, g = 12 mm).

gear-shaped patterns started to form much earlier (e.g. at t = 1–2 mins for $\sigma_i=284~\mu\text{S}$ —759 μS). With increased plasma ignition time, the gears started to disappear and were replaced by dots around the circumference. These structures changed to dotted rings, rings, overlapped rings, or star-shaped structures between 1015-4820 μS . For $\sigma_i=4820~\mu\text{S}$, the discharge started with a ring-shaped pattern. The ring around the circumference slowly started to disappear and after t = 5 mins, a star-shaped pattern started to form. The final conductance after 10 mins of plasma exposure was 5150 μS and it was higher by 6.85% w.r.t. the initial liquid conductance.

The gradual increment of σ_i in figure 2 reveal several interesting features. Firstly, it is interesting to note a sudden change of irregular shaped patterns to different types of patterns at the plasma-liquid interface. Initial charge buildup can play an important role in the formation of these patterns through the formation of electric double layers near the surface. Electric double layers usually separate plasmas with different properties [23–25]. They could occur at the interface between a gaseous plasma and a liquid electrolyte [26]. As the current flows through the plasma-liquid interface, these double layers can affect the formation of complex patterns. Next, the formation of these structures follows specific trend. In figure 2, the transition takes place as: solid discs, spikes, dots, rings, double rings, and stars. These beautiful structures represent plasma-induced emission at the liquid-anode interfaceand are necessary to sustain the discharge current [5]. Also, in figure 2, it is observed that the diameter of these patterns reduces as the conductance of the liquid solution increases. Indeed, ions within the liquid solution travel to the attachment point in order to neutralize the incoming electron charge. At high conductance, there are more ions per unit volume to neutralize the incoming electrons. Because of this, the diameter of the patterns reduces in size.

The change in liquid conductance in figure 2 only takes place in an incremental manner, and the initial liquid conductance for some conditions almost overlap or are close to the final conductance obtained after 10 mins of plasma ignition. For example, $\sigma_i = 191.6~\mu\text{S}$ (in the third row) is close to the final conductance of 203 μS obtained with $\sigma_i = 1.8~\mu\text{S}$. Similarly, the final conductance (=757 μS) obtained with $\sigma_i = 568~\mu\text{S}$ (5th row) is close to $\sigma_i = 759~\mu\text{S}$ (in the 6th row). If conductance is the only factor influencing the formation of SOPs, the patterns at the same liquid conductivities should be similar. But, they are observed to be different. This suggests that there are other factors, in addition to liquid conductance that influence the formation of patterns.

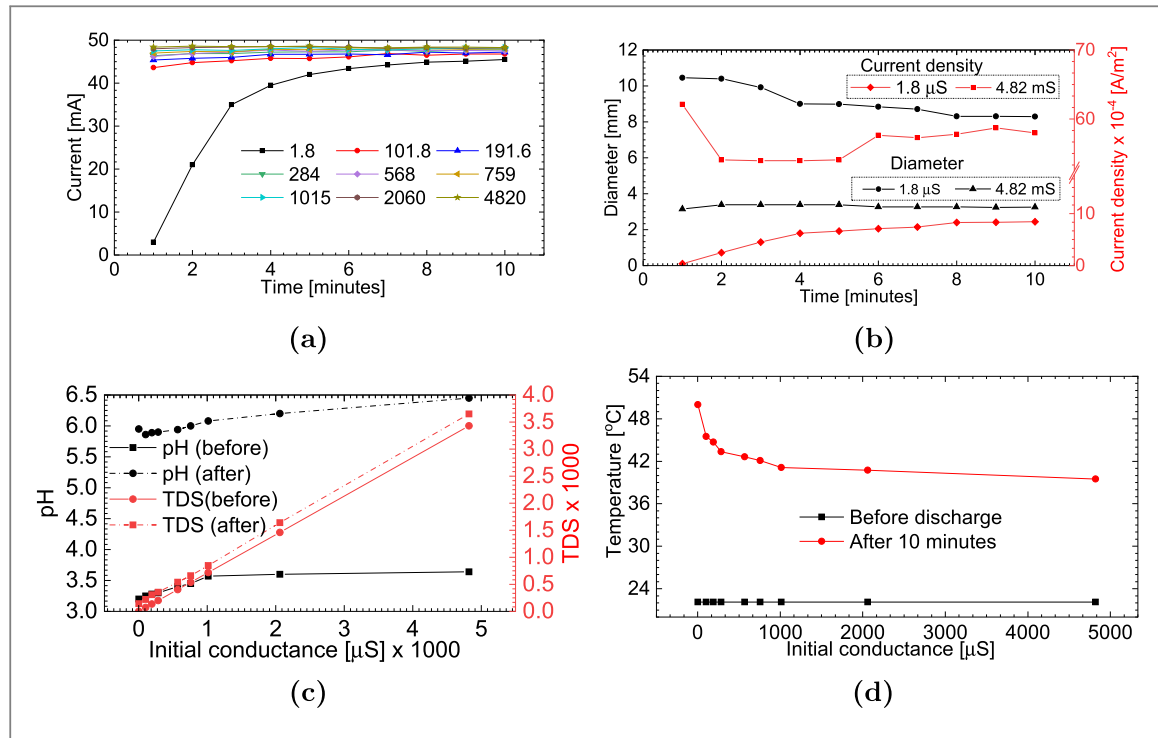


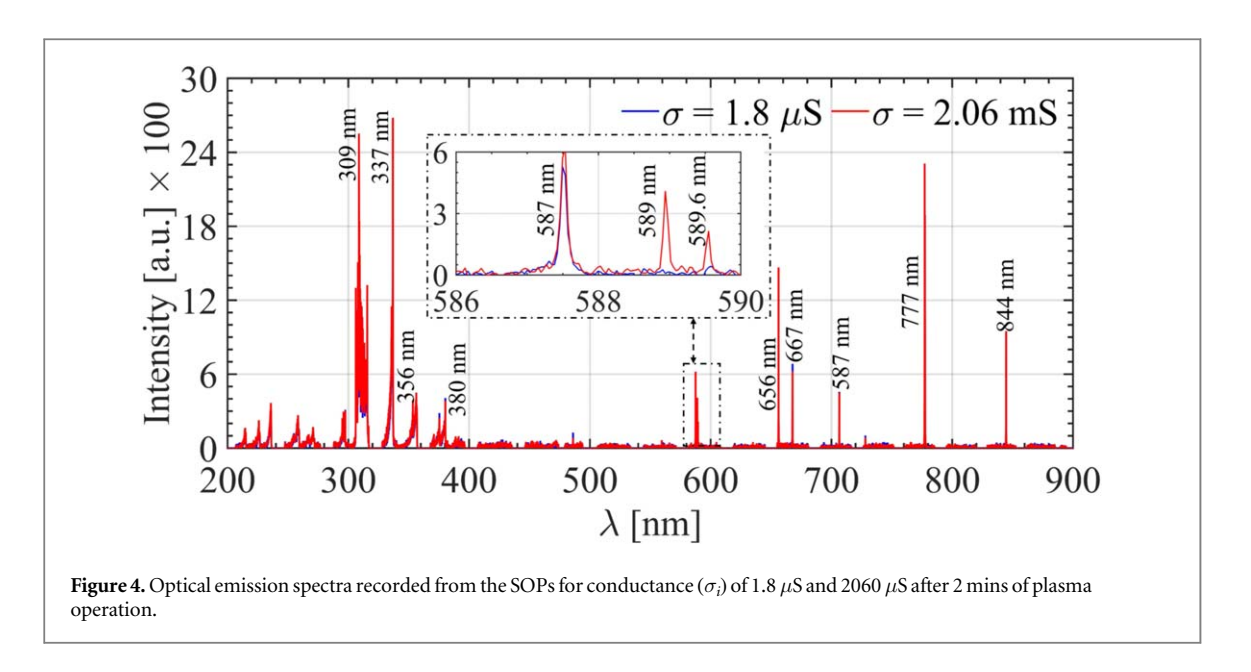
Figure 3. Measurement of (a) current; (b) diameter of SOPS and current density; (c) pH; and (d) liquid temperature before and after 10 mins of plasma treatment.

In order to understand what other variables influence the formation of SOPS, we measured the current, pH, total dissolved solutes (TDS), and liquid temperature. This is illustrated in figure 3. The change in current values at different plasma operation times is shown in figure 3(a). For distilled water ($\sigma_i = 1.8 \,\mu\text{S}$), the current increases linearly and slowly stabilizes. After 10 mins of plasma ignition, the measured value of current is \approx 47 mA. For other anode solutions, $\sigma_i = 101.8$ -4820 μ S, the current was stable at $\sigma_i = 46$ -48 mA. Distilled water contains less conductive ions, and ions tend to form through the ionization of ambient gas or water molecules by an increase of TDS. This process is seen to continue until there are sufficient ions for the conduction of electricity inside the solution.

The current values observed in figure 3(a) and the diameter of SOPs in figure 2 were further utilized to estimate the current density. This was performed for the liquid solution with the lowest and highest initial conductance ($\sigma_i = 1.8 \ \mu\text{S}$, $\sigma_i = 4820 \ \mu\text{S}$). As represented in figure 3(b), the diameter of SOPs for distilled water is observed to be three times higher than NaCl solution with $\sigma_i = 4820 \ \mu\text{S}$. For distilled water, the SOP diameter decreases from $\approx 10.45 \ \text{mm}$ to $\approx 8.29 \ \text{mm}$ as the plasma ignition time is increased from 1 to 10 mins. On the other hand, the diameter of SOPs for $\sigma_i = 4820 \ \mu\text{S}$ varies between 3.15 mm (t = 1 min) to 3.25 mm (t = 10 mins). The current density (=Current / Area of SOP) for $\sigma_i = 1.8 \ \mu\text{S}$ increases linearly from $\approx 3.49 \ \times 10^{-5} \ \text{A/m}^{-2}$ (t = 1 min) to $\approx 6.21 \times 10^{-4} \ \text{A/m}^{-2}$ (t = 4 mins). After that, it increases very slowly and remains constant $\approx 8 \times 10^{-4} \ \text{A/m}^{-2}$. The point at which the current density starts to become stable (i.e., t ≈ 4 -5 mins, figure 3(b)) corresponds to the point at which gear-shaped patterns start to form (figure 2). In contrast to this, the current density for $\sigma_i = 4820 \ \mu\text{S}$ varies between $\approx 6.21 \times 10^{-3} \ \text{A/m}^{-2}$ (t = 1 min) to $\approx 5.80 \times 10^{-3} \ \text{A/m}^{-2}$ (t = 10 mins) and patterns are observed since the start of the discharge. From figure 3(b), it can be inferred that the current density tries to remain constant when there are sufficient charge carriers for the conduction of current inside the liquid solution.

The increase in σ_i followed by subsequent plasma treatment also results in a change in the pH & TDS of the anode solution (figure 3(c)). The dissolved sodium salt slightly increases the pH of the liquid solution before plasma treatment, while the reactive species formed during the discharge process make the solution acidic. The pH of the 10 mins plasma activated solution was measured to be 3.25 and 3.64 (corresponding to initial pH of 5.95 and 6.45 respectively) for σ_i 's of 1.8 μ S and 4820 μ S, respectively. The most acidic solution (corresponding to $\sigma_i=1.8~\mu$ S) resulted in the highest increment of conductance (\approx 11200%). The corresponding increments for NaCl dissolved solutions were lower. These values for $\sigma_i=101.8~\mu$ S and $\sigma_i=4820~\mu$ S were obtained to be 266.4% and 6.85% respectively. These increments were accompanied by the linear increase in TDS and is a possible reason for the increment of final liquid conductance.

We also measured how the temperature (T) of the liquid solution changes during the pattern formation. The results are shown in figure 3(d). The initial temperatures of all liquid solutions were 22 °C. Distilled water (σ_i



= 1.8 μ S) resulted in the maximum increase of temperature (T after 10 mins = 50 °C) while the increase for higher conductive solutions was lower. The increase in temperature for $\sigma_i = 4820 \,\mu$ S after 10 mins of plasma treatment was \approx 17 °C).

The observations in figure 2 and 3 suggest that in addition to the liquid conductance (initially and after subsequent plasma exposure), the formation of SOPs could also be influenced by temperature, pH, ionic species present, etc. It is thus difficult to explain the mechanism of SOP formation based on conductance alone. The liquid anode solution at atmospheric pressure is chemically active due to the formation of several RONS and the local plasma effects (including chemical and thermal) induced at the attachment point slowly spread throughout the liquid through convection and diffusion mechanisms. Some of the previous publications have tried to explain the mechanism of pattern formation based on the reaction-diffusion mechanism [5, 22] as the patterns observed are similar to those observed in chemically active systems [27, 28]. But because of the complex interaction of the electrodynamic and hydrodynamic forces, additional investigations are necessary to understand their formation.

3.2. Optical emission spectroscopy

Optical emission spectroscopy is an important tool to identify the excited species formed during the discharge and the emission intensities from excited species could indicate several plasma parameters. In our study, we investigated whether the electrical conductance of the anode solution had any influence on the production of excited species at the SOP formation region.

Figure 4 shows the optical emission spectra (OES) recorded from the SOPs for the anode solutions with σ_i 's of 1.8 μ S and 2060 μ S respectively after 2 mins of plasma ignition. The solution with and without sodium salt was chosen to understand if there were any differences in the emission spectra. Both spectra show emissions from hydroxyl radical in the range of 309 nm, several bands of nitrogen second positive system (N₂ SPS) at 337 nm, 356 nm, 380 nm, etc., excited helium (587 nm, 667 nm, 706 nm), hydrogen alpha (656 nm) and atomic oxygen (777 nm and 844 nm) [29–31]. The anode solution with dissolved sodium salt showed emissions from sodium at 589 nm and 589.6 nm and these were not observed with distilled water anode. Emissions from hydroxyl radicals and hydrogen alpha appear due to the dissociation of water vapor molecules present in the interface region, while emissions from nitrogen second positive system and atomic oxygen are due to the dissociation of air molecules present in the ambient atmosphere [32, 33]. Helium emissions are due to the excitation of helium atoms fed through the working gas. The emission from sodium is due to the excitation of sodium atoms at the plasma-liquid interface [19, 34].

In the next step, we investigated the variation in the optical emission intensities from major reactive species (309 nm OH, 337 / 380 nm N_2 , 656 nm H- α , 777 nm O, and 667 nm He) as observed in the OES in figure 4. The spectra were recorded using Avantes spectrometer at an integration time of 100 ms and averaging of 10. These settings enabled recording of single spectrum every seconds. The results for a discharge duration of 10 mins for three anode solutions ($\sigma = 1.8 \ \mu S$, 101 μS and 2060 μS) are presented in figure 5. For $\sigma = 1.8 \ \mu S$ (figure 5(a)), the intensities from all species during the first 60 seconds are quite low. At \approx 1–2 mins, the intensities are seen to rise and fall. This is due to the unstable nature of the discharge as also observed at \approx 1–2 mins (figure 2). After 2 mins, the intensities from OH and excited N_2 (309 nm & 337 nm) slowly start to decrease while the emission from

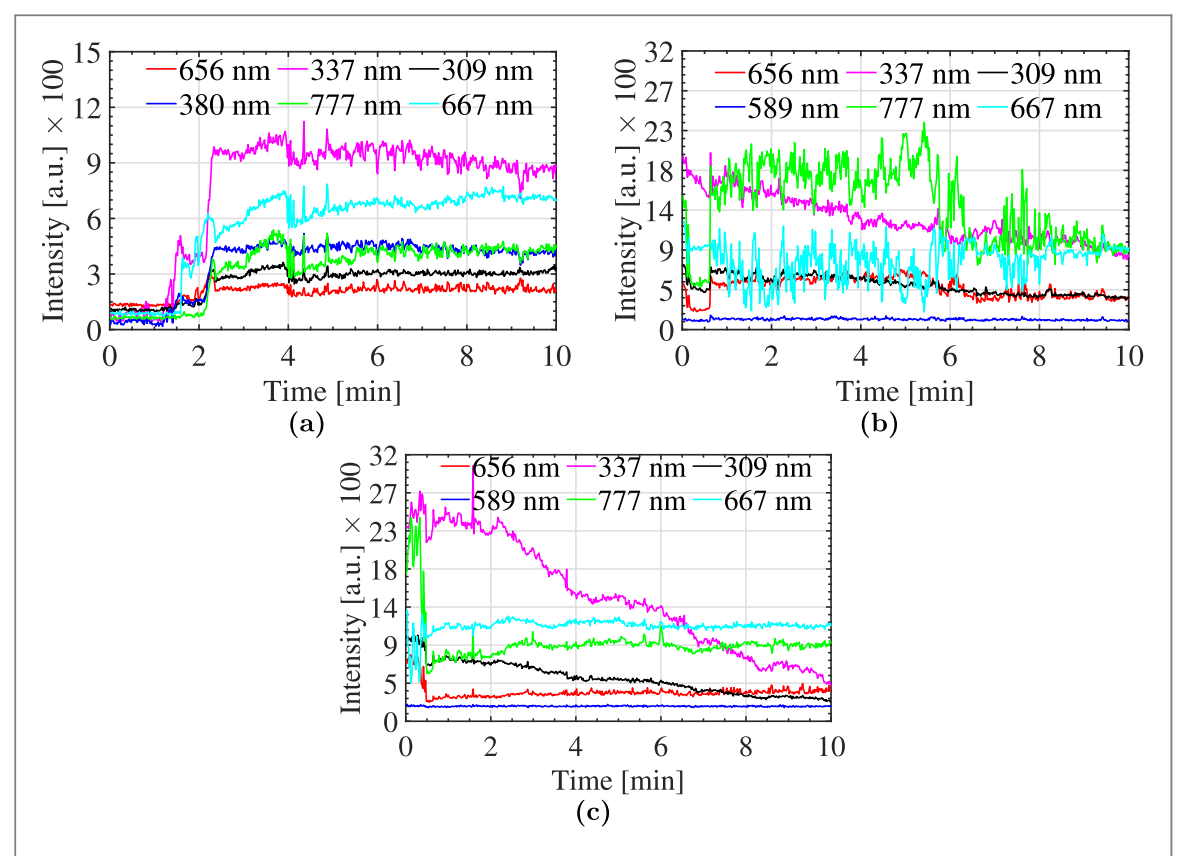


Figure 5. Variation in optical emission intensities from 309 nm OH, 337 / 380 nm N_2 , 656 nm H- α , 777 nm O, and 667 nm He for anode solutions of initial conductance - (a) 1.8 μ S, (b) 101 μ S and (c) 2060 μ S.

other species remains constant. The decrease in intensities from OH and excited N_2 is more obvious when the conductivity of the anode solution is increased (figures 5(b), 5(c)). With higher conductive solutions, the intensities from selected species appear immediately as soon as the discharge is on and this also correlates the immediate formation of SOPs in figure 2. The emissions from 656 nm H- α , 777 nm O, 667 nm He and 589 nm Na increase or remain constant for the total duration of the discharge.

The observations in figure 5 suggest that there must be a mechanism to balance the decrease in OH and N_2 species concentration through the formation of SOPs. The formation mechanism of OH and N_2 in atmospheric pressure plasma jets with liquid targets is well known [4, 33]. However, for plasmas generated above liquid-anode solutions, the liquid electrolyte could dissociate through electrolysis as:

$$H_2O \rightleftharpoons H^+ + OH^- (R1)$$

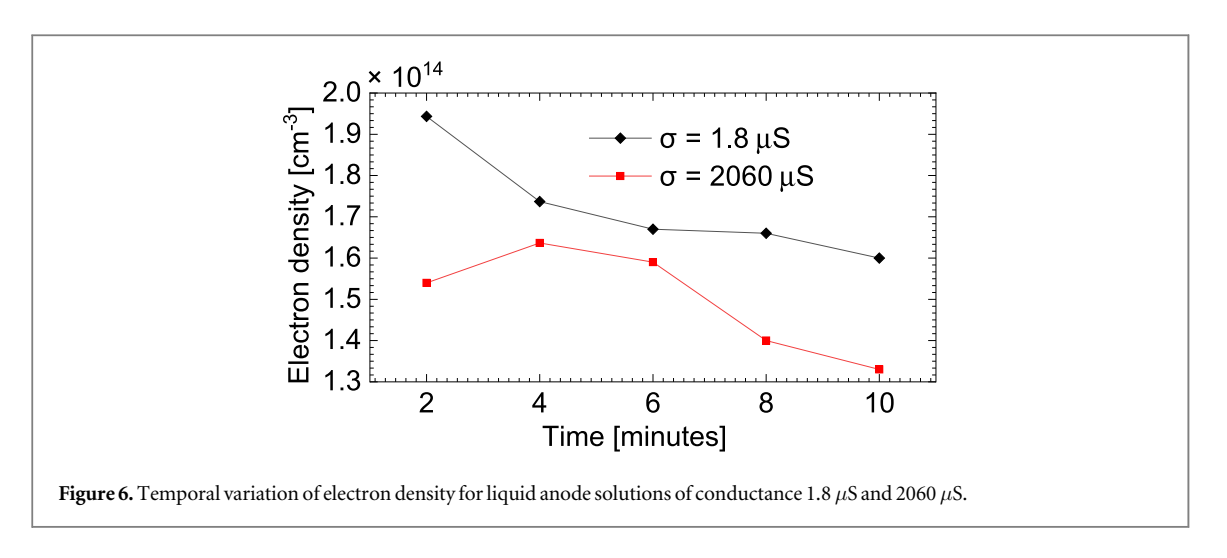
NaCl $\rightleftharpoons Na^+ + Cl^- (R2)$

The anions formed during this process move towards the anode, while the cations move towards the liquid-interface where the free or solvated electrons reduce them into stable atoms as:

$$H^+ + e^- \rightarrow H (R3)$$

 $Na^+ + e^- \rightarrow Na (R4)$

The nascent hydrogen and sodium atom formed in (R3)-(R4) could go into the discharge region above the water-interface and could be further excited/dissociated by electron impact. This mechanism results in the emission of light at 656 nm and 589 nm from H- α and sodium respectively as observed in the optical emission spectrum. This suggests that electrons at the plasma-water interface play an important role to reduce the cations and also to excite/ionize them. A plot of the electron density (n_e) obtained using the method of Stark broadening [35] for liquid anode solutions of conductance 1.8 μ S and 2060 μ S is shown in figure 6. With increasing time, we observed that the rotational temperature kept on increasing and this resulted in the decrease of electron density. The electron density for $\sigma_i = 1.8 \,\mu$ S reduced from 1.54×10 ¹⁴ cm⁻³ to 1.33×10 ¹⁴ cm⁻³ as the plasma was operated from 1-10 mins. A similar trend was observed for $\sigma_i = 2060 \,\mu$ S with a corresponding decrease in electron density from 1.94×10 ¹⁴ cm⁻³ to 1.60×10 ¹⁴ cm⁻³. In atmospheric pressure plasmas, energetic electrons also play a key role in the excitation/dissociation of ambient air/water molecules which could result in the formation of short-lived species such as OH, N₂⁺, etc. Since, the source electrons participate either in the reduction of cations formed at the plasma-water interface or excite/ionize them and their concentration decreases with time, the collisions with ambient water and nitrogen molecules are also reduced which results in the decrease of intensities from 309nm OH and N₂ SPS.



4. Conclusions

In conclusion, we investigated the role of initial liquid conductance on the temporal evolution of selforganization patterns at the plasma-liquid interface. With less conductive solutions, the formation of patterns was not realized immediately after discharge ignition and the discharge at the plasma-liquid interface was very unstable. With increasing liquid conductance, the formation of plasma was stabilized and formation of patterns took place. With enough ions in the electrolyte solution, i.e., higher liquid conductance, the current became stable, and the patterns formed as soon as the discharge was ignited. Patterns with specific trends (solid discs, spikes, dots, rings, double rings, and stars) were observed with gradual increment of initial liquid conductance up to 4820μ S. We also investigated the change in liquid properties due to SOP formation at the interface. The pH of the liquid solution changed to acidic, the temperature of the bulk of the liquid doubled, and the total dissolved solutes significantly increased as a result of SOP formation until ten minutes. Investigations through optical emission spectroscopy showed that emissions from short-lived reactive species mainly hydroxyl radical and excited nitrogen decreased while the decrease in the intensities from other excited species such as atomic oxygen, hydrogen alpha, excited sodium, etc were not realized. The decrease in the emissions from hydroxyl radical and excited nitrogen was accompanied by the decrease in electron density at the plasma-water interface. Our observations provide additional evidence to verify that cations formed within the anode solution interact with the electrons at the plasma-liquid interface and result in the formation of self-organized patterns through electrochemical reactions.

Acknowledgments

This work was supported by the NSF EPSCOR RII-Track-1 Cooperative Agreement OIA-2148653 and DOE DE-SC0021391. Any opinions, findings, conclusions, or recommendations expressed in the material are those of the author(s) and do not necessarily reflect the views of the National Science Foundation.

Data availability statement

All data that support the findings of this study are included within the article.

ORCID iDs

Bhagirath Ghimire https://orcid.org/0000-0002-5243-8528 Vladimir I Kolobov https://orcid.org/0000-0002-6197-3258 Kunning G Xu https://orcid.org/0000-0002-1249-0380

References

- [1] Chen Z, Xu R-G, Chen P and Wang Q 2020 Potential agricultural and biomedical applications of cold atmospheric plasma-activated liquids with self-organized patterns formed at the interface *IEEE Trans. Plasma Sci.* 48 3455
- [2] Chen Z, Zhang S, Levchenko I, Beilis I I and Keidar M 2018 In vitro demonstration of cancer inhibiting properties from stratified selforganized plasma-liquid interface Sci. Rep. 7 12163

[3] Shirai N, Uchida S and Tochikubo F 2014 Synthesis of metal nanoparticles by dual plasma electrolysis using atmospheric dc glow discharge in contact with liquid Japan. J. Appl. Phys. 53 046202

- [4] Bruggeman P J et al 2016 Plasma-liquid interactions: a review and roadmap Plasma Sources Sci. Technol. 25 053002
- [5] Foster J E, Kovach Y E, Lai J and Garcia M C 2020 Self-organization in 1 atm DC glows with liquid anodes: current understanding and potential applications *Plasma Sources Sci. Technol.* **29** 034004
- [6] Trelles JP 2013 Formation of self-organized anode patterns in arc discharge simulations Plasma Sources Sci. Technol. 22 025017
- [7] Trelles J P 2016 Pattern formation and self-organization in plasmas interacting with surfaces J. Phys. D: Appl. Phys. 49 393002
- [8] Kolobov VI and Golubovskii YB 2022 The principle of minimal power Plasma Sources Sci. Technol. 31 094003
- [9] Levko D, Arslanbekov R R and Kolobov V I 2019 Multi-scale dynamics of atmospheric-pressure discharges ignited over liquid electrodes J. Appl. Phys. 127 043301
- [10] Diamond J, Hamdan A, Profili J and Margot J 2020 Time and space-resolved imaging of an AC air discharge in contact with water J. Phys. D: Appl. Phys. 53 425209
- [11] Shirai N, Nakazawa M, Ibuka S and Ishii S 2008 Electrolyte-Cathode Atmospheric glow discharge with wide-gap operation using miniature gas flow IEEE Trans. Plasma Sci. 36 1160
- [12] Shirai N, Ibuka S and Ishii S 2009 Self-organization pattern in the anode spot of an atmospheric glow microdischarge using an electrolyte anode and axial miniature helium flow *Applied Physics Express* 2 036001
- [13] Shirai N, Uchida S, Tochikubo F and Ishii S 2011 Self-organized anode pattern on surface of liquid or metal anode in atmospheric DC glow discharges IEEE Trans. Plasma Sci. 39 2652
- [14] Shirai N, Nakazawa M, Ibuka S and Ishii S 2009 Atmospheric DC glow microplasmas using miniature gas flow and electrolyte cathode Japan. J. Appl. Phys. 48 036002
- [15] Shirai N, Ichinose K, Uchida S and Tochikubo F 2011 Influence of liquid temperature on the characteristics of an atmospheric dc glow discharge using a liquid electrode with a miniature helium flow Plasma Sources Sci. Technol. 20 034013
- [16] Shirai N, Uchida S and Tochikubo F 2014 Influence of oxygen gas on characteristics of self-organized luminous pattern formation observed in an atmospheric dc glow discharge using a liquid electrode Plasma Sources Sci. Technol. 23 054010
- [17] Li X, Kang P, Gao K, Zhou S, Wu K and Jia P 2020 Diffuse and spotted anode layers in an atmospheric pressure glow discharge Plasma Processes Polym. 17 1900223
- [18] Zhang S and Dufour T 2018 Self-organized patterns by a DC pin liquid anode discharge in ambient air: Effect of liquid types on formation Phys. Plasmas 25 073502
- [19] Srivastava T, Simeni M S, Nayak G and Bruggeman P J 2022 Self-organized patterns at the plasma-liquid anode interface in a helium glow discharge: temporal development and mechanisms *Plasma Sources Sci. Technol.* 31 085010
- [20] Kovach Y E, Garcia M C and Foster J E 2021 The variation in self-organized anode plasma pattern structure with solution electrolyte type in 1 atm DC glow discharge *Plasma Sources Sci. Technol.* 30 015007
- [21] Islamov R S and Golamov E N 1998 Numerical simulation of axisymmetric anode spot formation in glow discharge at elevated pressure IEEE Trans. Plasma Sci. 267
- [22] Rumbach P, Lindsay A E and Go D B 2019 Turing patterns on a plasma-liquid interface Plasma Sources Sci. Technol. 28 105014
- [23] Golubovskii Y B, Kolobov V I and Khavat S K 1990 ANODE DOMAIN OF WEAK-CURRENT GLOW-DISCHARGE AT LOW AND HIGH-PRESSURES Zhurnal Tekhnicheskoi Fiziki 60 179–82
- [24] Khlyustova A and Maksimov A 2013 Double electrical layer at the plasma-solution interface Contrib. Plasma Phys. 53 481
- [25] Kolobov V I 2013 Advances in electron kinetics and theory of gas discharges *Phys. Plasmas* **20** 101610
- [26] Bruggeman P J et al 2021 Plasma-driven solution electrolysis J. Appl. Phys. 129 200902
- [27] Horvath J, Szalai I and De Kepper P 2009 An experimental design method leading to chemical turing patterns Science 324 772
- [28] Gray P and Scott S K 1983 Autocatalytic reactions in the isothermal, continuous stirred tank reactor: Isolas and other forms of multistability *Chem. Eng. Sci.* 38 29
- [29] Clement F, Dauge C, Svarnas P, Gazeli K, Noel C and Belmonte T 2013 Multiple solutions in the theory of dc glow discharges *Plasma Sources Sci. Technol.* 22 025020
- [30] Ghimire B et al 2021 Enhancement of hydrogen peroxide production from an atmospheric pressure argon plasma jet and implications to the antibacterial activity of plasma activated water Plasma Sources Sci. Technol. 30 035009
- [31] Sarani A, Nikiforov AY and Leys C 2010 Atmospheric pressure plasma jet in Ar and Ar/H2O mixtures: Optical emission spectroscopy and temperature measurements Phys. Plasmas 17 063504
- [32] Ghimire B, Lamichhane P, Sup J, Booki L, Ramhari M, Klaus-Dieter Weltmann P and Choi E H 2019 An atmospheric pressure plasma jet operated by injecting natural air *Appl. Phys. Lett.* 113 194101
- [33] Ghimire B, Sornsakdanuphap J, Hong Y J, Uhm H S, Weltmann K D and Choi E H 2017 The effect of the gap distance between an atmospheric-pressure plasma jet nozzle and liquid surface on OH and N2 species concentrations *Phys. Plasmas* 18 073502
- [34] García M C, Kovach Y E and Foster J E 2019 Optical emission spectroscopy investigation of a 1-atm DC glow discharge with liquid anode and associated self-organization patterns *IEEE Trans. Plasma Sci.* 47 3214
- [35] Ghimire B, Briggs EF, Sysoeva TA, Mayo JA and Xu KG 2023 Contrasting the characteristics of atmospheric pressure plasma jets operated with single and double dielectric material: physicochemical characteristics and application to bacterial killing *J. Phys. D: Appl. Phys.* 56 085205